Chemical Engineering Journal 481 (2024) 148469

Contents lists available at ScienceDirect

Chemical Engineering Journal

journal homepage: www.elsevier.com/locate/cej

Heat transfer intensification in compact tubular reactors with cellular internals: A pilot-scale assessment of highly conductive packed-POCS with skin applied to the Fischer-Tropsch synthesis

Carlo Giorgio Visconti, Martino Panzeri, Gianpiero Groppi, Enrico Tronconi *

Politecnico di Milano, Dipartimento di Energia, Laboratory of Catalysis and Catalytic Processes, Via La Masa 34, Milano 20156, Italy

ARTICLE INFO

Keywords:
Process intensification
Heat management
Compact reactors
Structured internals
POCS
Fischer-Tropsch

ABSTRACT

Heat management poses severe constraints when designing non-adiabatic multi-tubular packed-bed reactors for strongly exothermic or endothermic catalytic processes. The exploitation of conduction in the solid matrix of engineered continuous internals (e.g., honeycomb monoliths, open-cell foams, periodic open-cell structures) as a heat transfer mechanism alternative, or possibly additional, to fluid-phase convection, is a promising strategy to relax some of these constraints, offering new opportunities for the intensification of catalytic reactors. Preliminary experimental data and modelling studies show that this is particularly true for compact-scale applications, when conductive internals are packed with catalyst micro-pellets. In this work, through pilot-scale testing, we show that overall heat transfer coefficients as high as 1300 $W/m^2/K$ can be achieved in periodic open-cell structures (POCS) made of a highly conductive aluminium alloy, 3D printed with an external continuous skin and packed with 300–400 μm catalyst micro-pellets. To this aim, a Fischer-Tropsch experimental campaign has been carried out in a pilot-scale rig, using an established 20 wt% Co/Al_2O_3 catalyst formulation and a tubular reactor (28.80 mm I.D., 20 cm catalyst bed length) externally cooled with an isothermal diathermic oil. Thanks to the outstanding heat transfer properties of the packed-POCS reactor, by progressively increasing the oil temperature from 180 °C to 225 °C, once-through CO conversions as high as 70 % have been measured at gas hourly space velocities exceeding 4000 $cm^3(STP)/h/g_{cat}$, resulting in C_5+ yields in excess of 0.35 $g/h/g_{cat}$, with a CH_4 selectivity always below 15 %. Such performances, made possible by the intensified heat management granted by the adopted reactor internals, are among the best ever reported for a compact-scale Fischer-Tropsch tubular reactor.

1. Introduction

Process intensification is one of the 21st century keywords of heterogeneous catalysis and chemical engineering. After a century mostly dedicated to the development of novel chemical processes, often relying on solid catalysts to synthesize new molecules, in the last 20 years attention has been devoted indeed to optimize existing processes in order to substantially increase their atomic and energy efficiency, while reducing their cost and environmental impact.

Considering that the main industrial heterogeneous catalytic reactions for energy conversion (e.g. steam methane reforming, hydrogenation and dehydrogenation processes) and chemicals production (e.g. selective oxidations) are carried out in fixed-bed tubular reactors loaded with randomly packed catalyst pellets, whose operation is intrinsically limited by slow heat removal/supply, it is not surprising that major efforts have been devoted in the process industry to intensify catalytic reactors for non-adiabatic processes [1,2].

As pointed out in [3], after a tremendously successful commercial application to the control of automotive and power stations emissions in the 1980s, starting in the mid-90s' [4], structured catalysts have been proposed as a potential alternative to packed-bed reactors also in the process industry [5]. In these catalysts, the active phase material was no longer dispersed on pelletized supports, but rather washcoated onto a spatially structured substrate pre-shaped in the form of monolithic honeycombs [6,7]. The idea was that of exploiting the high void fractions of such substrates, combined with the laminar flow prevailing in their parallel channels, to enable substantial reduction of the pressure drop with respect to conventional packed beds of catalyst pellets. Also,

* Corresponding author.
E-mail address: enrico.tronconi@polimi.it (E. Tronconi).

https://doi.org/10.1016/j.cej.2023.148469
Received 7 June 2023; Received in revised form 8 December 2023; Accepted 29 December 2023
Available online 30 December 2023

the large geometrical surface areas and the thin catalyst layers were considered novel strategies to diminish mass transfer limitations.

In spite of these premises, the success of structured catalysts was limited in the first decade of '00s [3] due to: (i) the modest inventory of catalytically active phase in a washcoated catalyst, which is critical for the reactions under kinetic control usually met in processes for chemicals production or energy conversion; (ii) the insulating behaviour of the honeycomb monolith substrates available on the market, which severely limits the control of temperature in non-adiabatic catalytic processes.

In 2004, some of us, in collaboration with Corning [8], showed that the thermal management issue can be solved, and even made much more effective than in packed-beds, by using highly thermally conductive structured substrates, such as honeycomb monoliths made of aluminium alloys. Under these circumstances, indeed, solid phase conduction can be even more effective than gas phase convection. Still, however, structured reactors were strongly limited by the low catalyst inventory in the reactor [9,10]. The situation did not significantly change when highly-conductive open-cell foams were proposed as an alternative to honeycombs, despite the higher specific surface granted by this innovative structured substrate [11,12].

Due to the aforementioned limits of multitubular packed-bed reactors – pushed by the strong demand of process intensification – alternative solutions were proposed starting from year 2000, based on the adoption of microchannel catalytic reactors [13–15]. New companies such as Velocys and CompactGTL were created to deploy such technologies.

Things for multitubular reactors changed when the adoption of highly conductive structured inserts, packed with catalyst micro-pellets, was proposed for compact-scale non-adiabatic processes [16,17]. Following a decade during which washcoating was considered the only method to exploit structured substrates in catalysis, in 2010 we claimed in fact that packing the catalyst within highly conductive structured honeycomb monoliths was an effective strategy to maximize both the inventory of catalyst in the reactor and the effective thermal conductivity, while allowing, at the same time to retain: (i) the typical pelletized catalyst design; (ii) the established packed configuration of tubular reactors; and (iii) the conventional industrial procedures for catalyst loading and unloading. According to this concept, the highly conductive monolith is no more a substrate for the catalyst, but becomes a conductive structured reactor internal, inside which a bed of micropellets is randomly packed.

Starting in the same years, other research groups proposed different solutions, such as conductive microfibrous structures [18,19,2], knitted wires, open-cell foams, cross flow structures [20,21] and cooling inserts [22] as alternatives to conductive honeycomb monoliths. Some of these solutions have been studied by our group as well. In particular, starting from 2015, the concept of packed structured reactors was extended to cellular materials with interconnected cavities, i.e. open-cell foams, OCF [23], and periodic-open-cell-structures, POCS [24]. For both these cellular structures, some of us have theoretically shown and experimentally demonstrated [25,26] that the heat transfer takes advantage of both the conduction within the 3D continuous structure, which is a heat transfer mechanism dominating in the bulk of the bed, and the convection in the catalyst bed packed in the open cells, which plays a key role at the boundary between bed and tube wall.

POCS, proposed for the first time in 2011 [27] with the name "periodic open-cell foams" and then re-named as "periodic open-cell structures" [28], were found particularly promising. In fact, POCS can be engineered and tailored by Computer-Aided Design (CAD) techniques and then fabricated by modern additive manufacturing methods such as 3D printing [29], overcoming some drawbacks associated with the OCF manufacturing processes, which do not allow a fine control of the geometry. Among the tailored properties of POCS, the uniform strut shape, the tuneable void fraction/relative density, the engineered morphology (3D geometry of the unit cell, isotropy vs. anisotropy, etc.) and the possibility to use many different manufacturing materials [30], are most important.

Notably, many of the aforementioned structured reactor technologies have been developed specifically for the low-temperature Fischer-Tropsch synthesis (FTS), a strongly exothermic catalytic reaction where a 2/1 mixture of H_2 and CO (synthesis gas) is converted into long chain hydrocarbons (-(CH_2)-$_n$) over a cobalt-based catalyst (Eq. (1)):

$$n\,CO + 2n\,H_2 \rightarrow -(CH_2)_n- + n\,H_2O \qquad \Delta H_R^0 = -167\,kJ/mol \tag{1}$$

In this reaction, heat management is particularly critical since it strongly affects the reaction rate (the kinetics has a very high activation energy [31–33]), the reaction selectivity (which shifts towards the undesired low molecular weight species at high temperatures [34]), as well as the catalyst stability [21].

In 2018, using a laboratory-scale tubular reactor loaded with a packed-foam or with a packed-bed with the same catalyst density (catalyst mass per unit reactor volume), through comparative testing, some of us have shown [35] that a conductive packed-OCF made of 6000 series aluminium-alloy allows to run the FTS at CO conversion levels and heat duties which are not accessible using the a conventional randomly packed-bed. Due to the simplicity of the adopted setup, however, no quantitative information could be derived on the enhancement of the overall heat transfer coefficient granted by the presence of the conductive foams in the reactor. Nevertheless, we were able to show that the improved performances measured in the presence of the Al-foam were not simply due to the presence of some metallic diluent in the reactor, but were due to the continuity of the metal struts transferring heat in the radial direction of the reactor [36].

A couple of years later, using the same laboratory plant, the performances of the packed-OCF have been then compared to those of a packed-POCS with a similar relative density and made of a very similar Al-alloy [24]. Through a direct comparison, we have shown that packed-POCS further enhances the heat transfer: this has been ascribed to the regular and more controlled geometry of the POCS structure, which was specifically engineered to intensify the internal thermal conductivity, and to the improved contact of the 3D-printed structure with the reactor wall, which governs the wall heat transfer coefficient. Again, however, no quantitative indication on the overall heat transfer coefficient were derived, due to limitations in the experimental setup which did not enable an accurate control of the reactor wall temperature.

To further boost the performances of the packed-POCS, very recently we have designed, manufactured and tested two POCS made of the same Al-alloy and with the same geometry (cell type and size, relative density), the only difference being the presence of a continuous metal "skin" on the outer surface of the two POCS [37]. Experiments at the lab scale have shown that the skin results in a limited loss of catalyst inventory, while granting a better thermal contact with the reactor walls, a greater mechanical resistance and the possibility to load or offload the POCS with the catalyst in the reactor tubes like a cartridge.

To gain quantitative information on the overall heat transfer coefficients in packed tubular reactors loaded with highly conductive POCS with skin, while demonstrating at higher technology readiness level (TRL) the possibility to operate compact scale tubular reactors for the Fischer-Tropsch synthesis based on this technology, in this work packed-POCS with skin, loaded with Co/γ-Al_2O_3 micropellets, have been tested in a fully instrumented pilot-scale tubular reactor, externally cooled with diathermic oil. We show that the adopted configuration grants exceptional overall heat transfer coefficients, paving the way to the development of compact multi-tubular reactors for the Fischer-Tropsch synthesis (and for other non-adiabatic catalytic process) which are unfeasible with the current technologies.

2. Experimental

2.1. Structured internals

POCS with solid struts made of $AlSi_{10}Mg$ alloy (composition: 88.55–90.80 wt% Al, 9–11 wt% Si, 0.2–0.45 wt% Mg, bulk thermal conductivity = 150 W/m/K), manufactured by AIDRO S.r.L. (Italy) using a Renishaw AM250 3D printer exploiting the Selective Laser Melting technology, were tested (Fig. 1). The customized POCS geometry, engineered in our laboratories and designed with the OpenSCAD free software by repeating the unit cell in all spatial dimensions, is characterized by diamond cells with a nominal diameter (d_C, defined as reported in [38]) of 3.00 mm, with struts (circular cross section) 0.70 mm thick (d_S), forming a cellular material with a 27.00 mm nominal outer diameter (od). Notably, as reported in [38], once two geometrical parameters of the POCS are defined (d_C and d_S in this case), the other four geometrical parameters of the POCS, namely, the strut length, the surface area, the porosity (or its complement, the relative density), and the mean window diameter (d_W), are set.

An outer metallic "skin" with a 0.90 mm nominal thickness (t_{OS}) was printed on the periphery of the cellular structure, resulting, after polishing the 3D printed sample to increase the smoothness of the outer surface, in cylindric "POCS with skin" samples 99 mm long (L) and with a targeted outer diameter (OD) of 28.80 mm.

The POCS with skin samples were designed to include one axial through hole of 3.20 mm diameter (ID) along the centerline, allowing for the tight insertion of a stainless steel thermowell (with nominal outer diameter of 3.20 mm) protecting a sliding E-type multipoint (5 points) thermocouple for the measurement of the axial temperature profiles during the Fischer-Tropsch runs (cf. Section 2.2). To facilitate the 3D printing of the POCS with the central hole, as well as the thermowell insertion along the centerline of the POCS, an additional "internal skin" with a nominal thickness (t_{IS}) of 0.40 mm was printed between the central hole and the cellular structure.

The actual sizes of the POCS sample loaded in the reactor for the FTS runs were measured with a digital disk micrometer (Rupac model 2393050) and using images collected by a scanning electron microscope (SEM, Carl Zeiss Evo 50 EP). The volume of the tested POCS sample occupied by the metal struts (V_{MET}) was measured immersing the POCS sample in a cylinder filled with acetone and observing the level increase (acetone displacement experiments).

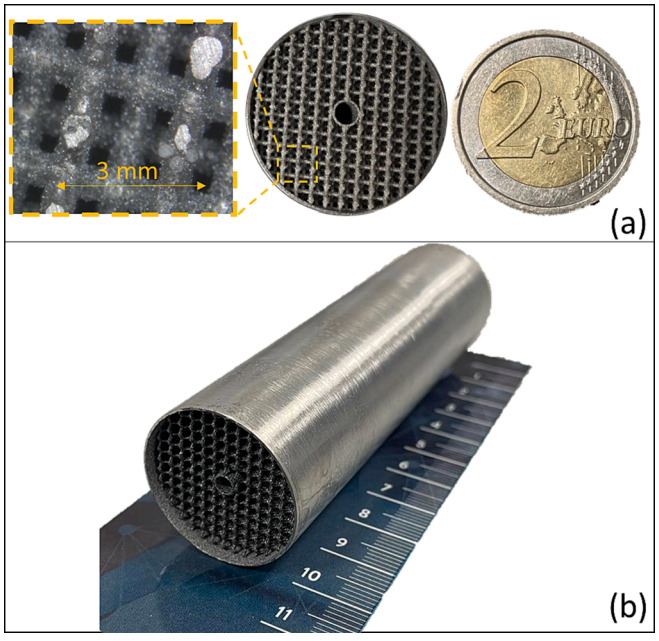

Fig. 1. (a) top view and (b) perspective view of the adopted POCS with skin, after the external polishing treatment.

2.2. Reactor

Two bare samples of POCS with skin (each 99.00 mm long) were loaded in a 316L stainless steel jacketed tubular reactor with an internal diameter (ID_R) of 28.80 mm (±0.05 mm, measured by a Carl Zeiss Accura II 3D coordinate measuring machine), obtained by reboring, a total length of 871 mm and a jacket opening of 4.68 mm, Fig. 2(a). The reactor, cooled with diathermic oil (Julabo Thermal H350) flowing counter-currently with respect to the reacting mixture, was operated downflow. Once loaded in the reactor, the POCS samples were fully filled with the Co/Al_2O_3 catalyst.

As shown in Fig. 2(b), the reactor was designed so to allow the loading of two POCS in its central part and the monitoring of the reactor skin temperature in correspondence to the inlet (z = 0 mm), the outlet (z = 200 mm) and along the entire length of the bed with a spatial resolution of 50 mm (z = 50, 100, 150 mm). To this aim, the reactor was equipped with 5 thermowells (1/4 in. O.D.) radially inserted in the jacket and welded on the tube skin (Fig. 2(c)). Within each thermowell, single point E-type thermocouples (1.00 mm O.D.) were installed, with the hot-joint located on the tip and the tip positioned at the very end of the thermowell. Two radial thermowells (1/4 in. O.D.) were also installed at z = −70 mm and z = 270 mm to measure the temperature of the diathermic oil flowing in the jacket upstream and downstream the catalyst bed (Fig. 2(d)). To the scope, two Pt100 thermoresistors were used.

A 316 L stainless steel thermowell (3.2 mm I.D., 0.25 mm thickness) crosses the entire length of the reactor along its centerline, allowing a multipoint E-type thermocouple (1.8 mm O.D.) to measure the temperature in the hottest point of the reactor. The adopted thermocouple was designed so to have the 5 hot-joints at axial positions corresponding to the position of the 5 thermowells used to read the skin temperature of the reactor. Through a fully-automated electrical actuator, this thermocouple can be slided vertically (±75 mm) in order to record the temperature profile of the catalytic bed with a 1 mm resolution.

The size of the reactor jacket, as well as the specification of the pump feeding the oil into the jacket, were selected so to ensure an external heat transfer coefficient in excess of 5 $kW/m^2/K$. This minimizes the heat transfer resistances between the tube wall and the coolant. Also, the pilot-plant engineering was done to allow a maximum temperature variation of the diathermic oil temperature below 0.5 °C, also granting a maximum deviation of the temperature of the diathermic oil within ± 0.1 °C from the setpoint value.

2.3. Pilot-plant configuration

The adopted pilot-plant, whose Front End Engineering Design (FEED) has been carried out within our group at Politecnico di Milano and the detailed Engineering, Procurement and Construction (EPC) by Process Integral Development Eng&Tech S.L. (a Micromeritics Company), is constituted by four sections: (i) gas feed; (ii) reaction; (iii) condensable product separation; (iv) on-line analysis of incondensable products.

The gas feed section consists of four different gas lines which feed nitrogen, hydrogen, carbon monoxide and a mixture of argon and oxygen (for catalyst post-run passivation) to the process. On each line, the same common elements are installed, including a filter, a pressure regulator, a mass flow controller, two actuated valves to open/close the feed line and isolate the mass flow controller, and a check valve. The CO line also has a carbonyl trap (filled with a 12 wt% $K/\gamma\text{-}Al_2O_3$ sorbent in trilobe shape and kept at 160 °C) to reduce iron carbonyls possibly present in CO to a concentration below 1 ppm, thus preventing the catalyst poisoning. After the feed gas mixing, the $H_2/CO/N_2$ mixture goes through a molecular sieve (13X type) trap, which retains particles

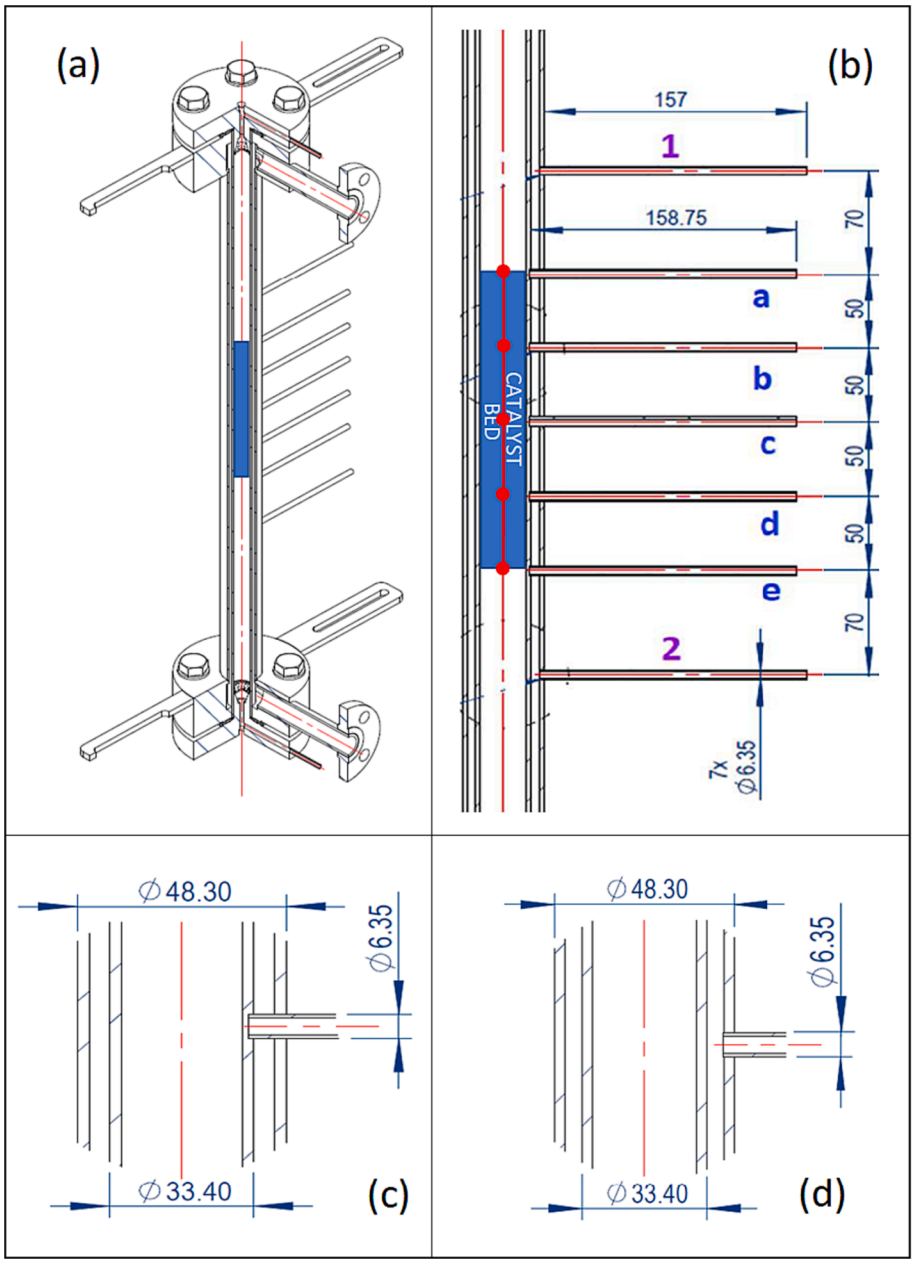

Fig. 2. (a) jacketed reactor – isometric projection; (b) location of radial thermowells with respect to the catalyst bed; (c) detail of the contact between skin thermowells (a,b,c,d,e) and the reactor wall; (d) detail of the contact between oil thermowells (1 and 2) and the reactor jacket. All the sizes are expressed in mm.

and moisture and acts as a static mixer. Then, this stream goes through an electric heater, where it is preheated to 180 °C before entering the reactor.

The reaction products are fed to a first phase separator, heated at 120 °C, through a traced line. In this L/V separator, condensed heavy hydrocarbons are separated from vaporized middle distillates, low molecular weight hydrocarbons and unconverted reactants. Through an automated control loop, the waxes collected in this separator are continuously evacuated and sent to a 10 L wax storage tank. Vaporized compounds leaving the L/V separator are cooled down in a shell and tube heat exchanger (flowing counter-currently to ethylene glycol at 0 °C) and reach a liquid/liquid/vapor three-phase separator, where an aqueous phase is removed from the bottom, an organic phase from the centre and light gases from the top. Aqueous and organic phases are collected in their respective condensate storage tanks, while incondensable gases are sent to a back-pressure regulator, followed by a gas flow meter and totalizer and then vented to the atmosphere.

Samples of the incondensable gases are periodically sent to the on-line analysis section, where CO and H_2 conversions, as well as the light hydrocarbon selectivity are assessed by on-line gas-chromatography using an Agilent 8890 refinery gas analyzer. To capture any possible instability of the catalyst reactivity, the composition of the tail gases was measured with a frequency of two analyses every hour.

2.4. Catalyst

Experiments were carried out using a 20 wt% cobalt supported catalyst, purchased from Soluciones Catalíticas IBERCAT S.L. According to the supplier's specifications, the catalyst was prepared using γ-Al_2O_3 (specific surface area = 250 m^2/g, average pore size = 66 Å, pore volume = 0.59 mL/g, nominal particle size (d_p) in the range 300–400 μm, packing density 650 kg/m^3) as support and loading cobalt on the support in a single impregnation step.

The particle size distribution (PSD) was assessed by both laser

granulometry using a CILAS 1180 instrument (Compagnie Industrielle des Lasers, Orléans, France), and the ImageJ software (version 1.53) analysing a scanning electron microscope (SEM) image taken with a Carl Zeiss Evo 50 EP instrument. SEM images were used also for the computation of PSD to confirm the measurements from laser granulometry analysis, thus preventing possible errors in its determination caused by agglomeration of catalyst particles during the laser analysis.

Due to the low d_p/d_W (vide infra), the catalyst was free-flowing in the POCS. Accordingly, the reactor was loaded with the two POCS first, and then the catalyst was poured within the structured internals.

2.5. Activity runs

The capability of the adopted POCS with skin to manage the heat produced by the strongly exothermic Fischer-Tropsch synthesis was assessed through experimental runs at different duties (cf. section 2.6), measuring the axial temperature profiles along the reactor centerline, as well as the skin temperature of the reactor.

To the scope, FTS runs were carried out at process conditions relevant to industrial operation: oil temperature between 180 and 230 °C, pressure between 15 and 25 barg, H_2/CO feed ratio of 2.1 mol/mol, 6 mol.% N_2 (Sapio, 99.999 mol.%) in the feed and gas hourly space velocities (GHSV) between 3500 and 6000 cm^3(STP)/h/g_{cat}. Changes in the oil temperature were carried out by setting temperature ramps of 0.03 °C/min so to limit excessive stresses for the catalyst. A full temperature profile of the catalyst bed was collected every 4 h so to verify the stability of the catalytic reactor.

Before admitting syngas to the reactor, the Co/Al_2O_3 catalyst was reduced in-situ flowing a 3/1 mol/mol mixture (400 NL/h) of H_2 (Sapio, 99.995 mol.%) and N_2 (Sapio, 99.999 mol.%) at 350 °C (heating rate = 3 °C/min from room temperature to 250 °C and 1 °C/min from 250 to 350 °C) and atmospheric pressure for 17 h.

Each run had a duration of at least 500 h, and every condition was tested for at least 12 h to check the system stability, especially in terms of sensitivity to the oil temperature. The stability was verified at all the investigated conditions, as demonstrated by the CO conversion varying less than 1 % in 12 h on a relative basis, and by the superimposed temperature profiles.

During the run, the reactor temperature was constantly monitored through the five readings of the axial multipoint thermocouple, the readings of the five skin thermocouples and the readings of the two Pt100 thermoresistors located in the oil jacket.

2.6. Assessment of the material and thermal performances of the structured reactor

Three Key-Performance Indicators (KPIs) were used to characterize the FTS reactivity, namely the CO conversion (χ_{CO}, Eq. (2)), the CH_4 selectivity (σ_{CH4}, Eq. (3)) and the C_5+ specific yield (Y_{C5+}, Eq. (4)).

$$\chi_{CO} = 1 - F_{CO}^{out}/F_{CO}^{in} \quad (2)$$

$$\sigma_{CH4} = F_{CH4}^{out}/\left(F_{CO}^{in} \bullet \chi_{CO}\right) \quad (3)$$

$$Y_{C5+} = F_{C5+}^{out}/(W_{cat} \bullet L) \quad (4)$$

Table 1
Characteristics of the adopted catalyst, reactor, POCS and of the packed-POCS catalyst bed.

Parameter	Symbol	Unit	Spec.	Experimental or calculated value	Note for "Experimental or calculated value"
Reactor internal diameter	ID_R	mm	28.80	28.80 ± 0.05	Measured with 3D coordinate measuring machine
POCS w/skin outside diameter	OD	mm	28.80	28.78 ± 0.01	Measured with micrometer
POCS w/skin inside diameter	ID	mm	3.20	3.33 ± 0.04	Measured from SEM images
POCS outside diameter excluding the skin	od	mm	27.00	27.05 ± 0.08	Measured from SEM images
POCS inside diameter including the skin	id	mm	4.00	3.86 ± 0.06	Measured from SEM images
Outer skin thickness	t_{OS}	mm	0.90	0.87	= (OD −od)/2
Inner skin thickness	t_{IS}	mm	0.40	0.27	= (id −ID)/2
POCS length	L	mm	99.00	99.00 ± 0.05	Measured with digital callipers
Cell diameter	d_C	mm	3.00	3.03 ± 0.06	Measured from SEM images
Strut diameter	d_S	mm	0.70	0.69 ± 0.04	Measured from SEM images
Window diameter	d_W	mm	1.63	1.66	Calculated as reported in [39]
Average pellet diameter	d_P	μm	300–400	337	Measured from laser granulometry
POCS w/skin solid volume	V_{MET}	cm^3	–	20 ± 2	Measured from acetone displacement experiments
Relative density of the POCS	RD_{POCS}	–	–	0.31	$= V_{MET}/(V_{OD}\text{-}V_{ID})$*
Void fraction (no packing)	ε_{POCS}	–	–	0.69	$= 1 - RD_{POCS}$
Void fraction (no packing) of the cellular structure only[a]	ε_S	–	–	0.78	$= \varepsilon_{POCS}(OD^2 - ID^2)/\left(od^2 - id^2\right)$
Relative density of the cellular structure only[a]	RD_S	–	–	0.22	$= 1 - \varepsilon_S$
Mass (no packing)	M_{POCS}	g	–	52.57 ± 0.01	Measured with scale
Packed catalyst mass	M_{CAT}	g	–	37.23 ± 0.01	Measured with scale
Packed catalyst density in empty cylinder	$\rho_{CAT,E}$	g/cm^3	–	0.94	Measured from catalyst loading experiments
Packed catalyst density inside the POCS	ρ_{CAT}	g/cm^3	–	0.67	$= M_{CAT}/(V_{od} - V_{id})$*
Packed catalyst density inside the reactor	$\rho_{CAT,R}$	g/cm^3	–	0.58	$= M_{CAT}/V_D$*
Catalyst pellet density	$\rho_{CAT,P}$	g/cm^3	–	1.50	$= \rho_{CAT,E}/(1–0.375\dagger)$
Specific[b] catalyst loading	W_{CAT}	g/cm	–	3.76	$= M_{CAT}/L$
Specific[b] catalyst volume[c]	V_{CAT}	cm^3/cm	–	2.50	$= W_{CAT}/\rho_{CAT,P}$
Catalyst volume fraction[d]	ξ	–	–	0.44	$= V_{CAT}L/(V_{od} - V_{id})$*
Void fraction (with packing)	$\varepsilon_{P\text{-}POCS}$	–	–	0.34	$= 1 - RD_S - \xi$
Packing relative density[e]	$RD_{PACKING}$	–	–	0.57	$= V_{CAT}L/(\varepsilon_S(V_{od} - V_{id}))$*
Packing porosity	$\varepsilon_{PACKING}$	–	–	0.43	$= 1 - RD_{PACKING}$
Window to pellet ratio	R	–	–	4.93	$= d_W/d_P$

[a]This value refers to the volume included between the outer and the inner skins. [b]per unit length. [c]volume or [d]fraction of total volume occupied by the catalyst pellets, excluding the voids between pellets. [e]fraction of the void volume in the POCS occupied by the catalyst pellets. *V_i (i = OD, ID, od, id, D) is defined as the volumes of the cylinders with diameter i and length L. †0.375 is the solid fraction of an ideal packed bed of pellets, according to Eq. (10).

In Eqs. (2) to (4), F_i^{in} and F_i^{out} are the inlet and the outlet molar flows of the i-species, respectively. In Eq. (4), W_{cat} is the specific mass of catalyst loaded in the reactor and L is the catalyst bed length (cf. Table 1).

The volumetric heat duty (Q_{vol}) released at each condition was calculated according to Eq. (5), where ΔH_R^0 is the standard reaction enthalpy (cf. Eq. (1)) and V the volume of the structured catalytic bed.

$$Q_{vol} = -F_{CO}^{in} \cdot \chi_{CO} \cdot \Delta H_R^0 / V \left[W/m^3\right] \quad (5)$$

In the same way, the heat flux (Q_{surf}) was computed according to Eq. (6), normalizing the reaction heat release by the lateral surface area of the structured catalytic bed (S_{lat}).

$$Q_{surf} = -F_{CO}^{in} \cdot \chi_{CO} \cdot \Delta H_R^0 / S_{lat} \left[W/m^2\right] \quad (6)$$

The overall radial temperature difference (ΔT_{ext}), defined as the difference between the average catalyst temperature on the centerline ($T_{cat,avg}$) and the average oil temperature ($T_{oil,avg}$), was computed starting from the temperature readings collected with a 1 mm resolution on the reactor axis (Eq. (7)).

$$\Delta T_{ext} = T_{cat,avg} - T_{oil,avg} \quad (7)$$

To this aim, the average temperature on the centerline was computed as mean average of the temperature measurements collected at axial coordinates (z) between 0 (catalyst bed inlet) and 200 mm (catalyst bed outlet), while the average oil temperature was computed as the mean average of the temperature measurements collected in the oil jacket, upstream (z = −75 mm) and downstream (z = 275 mm) the catalyst bed.

3. Results and discussion

3.1. Catalyst characterization

The particle size distributions (PSD) of the adopted catalyst, measured by laser granulometry and by software analysis of SEM images, are shown in Fig. 3(a and b), respectively. According to the laser granulometry measurement, apart from a minor fraction of particles, accounting for less than 3 vol% (5 wt%) of the catalyst loaded in the reactor, which have a diameter centered around 100 μm, particles have a monomodal PSD centered at a diameter of 337 μm (d_P). In particular, more than 84 vol% of the pellets have a diameter between 300 and 400 μm. The PSD obtained from the software analysis of the SEM image confirms the results from the previous analysis.

3.2. Packed POCS characterization

Table 1 lists the geometrical characteristics of the adopted POCS. Notably, experimentally measured OD, ID, od, id, t_{OS}, t_{IS}, L, d_C, d_S and d_W values are in good agreement with the nominal specifications, confirming the flexibility of the 3D printing technology based on selective laser melting to manufacture engineered structured internals for tubular reactors.

One of the key-parameters for the POCS is its outside diameter (OD). This value, in fact, together with the radial effective conductivity, controls the efficiency of the heat transfer between the POCS and the reactor wall. The average gap between the reactor wall and the POCS, determined as half of the difference between the reactor inside diameter (ID_R) and the POCS OD, is 10 μm at room temperature. This allowed an easy loading of the bare POCS with the skin in the reactor. Nevertheless, due to the differential thermal expansion coefficient of the aluminium alloy used to manufacture the POCS and the stainless steel used to manufacture the reactor, this gap is likely to be closed at the FTS process conditions, contributing to maximize the heat transfer between the structured internals and the reactor wall.

The cell and the strut diameters, equal to 3.03 and 0.69 mm respectively, resulted in the expected value of the void fraction ($\varepsilon_{POCS,theor}$) of 0.77, computed according to Eq. (8) [39]:

$$\varepsilon_{S,theor} = 1 - \frac{3\pi\sqrt{3}}{16\left(\frac{d_C\sqrt{3}}{4d_S}\right)^3}\left(\frac{d_C\sqrt{3}}{4d_S} + \frac{\sqrt{2}}{2}\left(\frac{1}{3} - \frac{\sqrt{3}}{2}\right)\right) \quad (8)$$

Such a value well matches the value of 0.78 computed when the POCS skins are not considered, as shown in Table 1. The corresponding relative density of the adopted POCS with skin samples (RD_{POCS}) is 0.31.

To completely fill the structured bed, containing 2 POCS, each one 99 mm long, 74.5 g of catalyst are used, corresponding to a catalyst volume fraction (ξ) of 0.44 and a residual void fraction ($\varepsilon_{P\text{-}POCS}$) of 0.34.

In a recent work by some of us [26], it has been shown that the packing density ($\varepsilon_{PACKING}$) of POCS (without the skin and without a hole

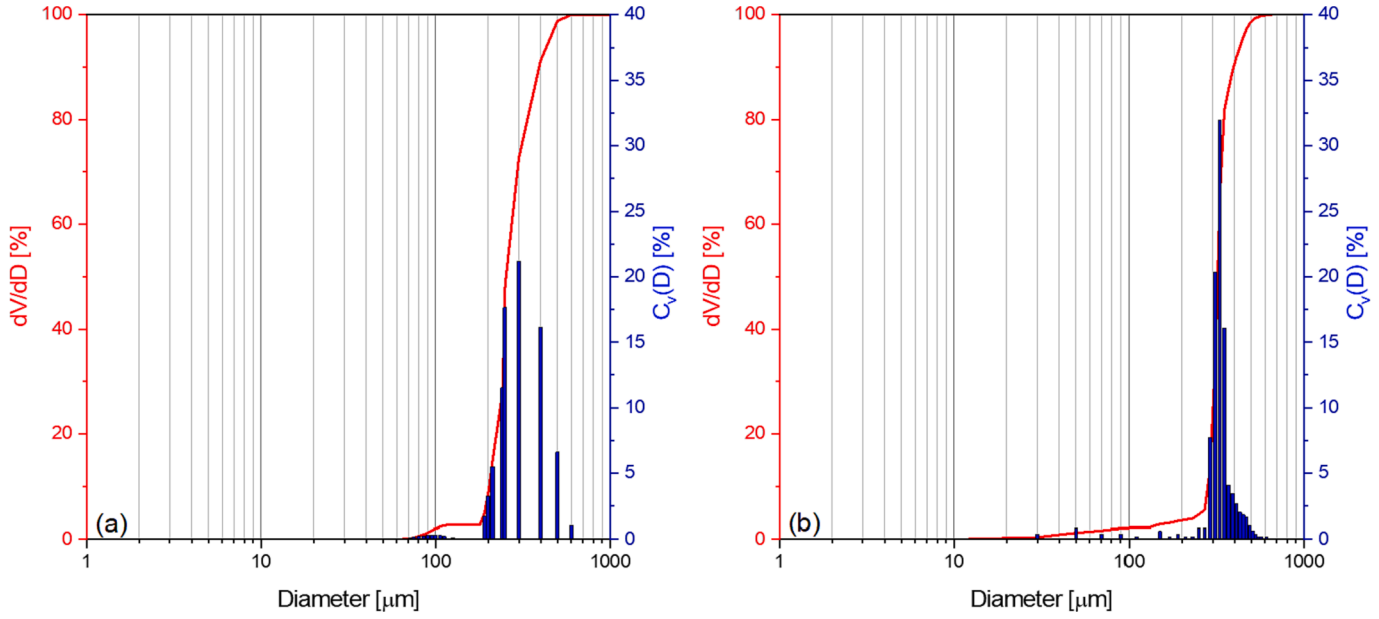

Fig. 3. Particle size distribution of the adopted catalyst, measured by (a) laser granulometry and (b) software analysis of SEM images. Left y-axis: cumulative volume distribution; right y-axis: differential number distribution.

on the centerline), is a function of the ratio (R) between the POCS window (d_W), computed with Eq. (9) starting from the POCS cell (d_C) and strut (d_S) diameters [39], and the catalyst pellet diameter (d_p), as summarized by Eq. (10).

$$d_W = \left(\frac{6\sqrt{3}}{\pi}\right)^{0.5}\left(\frac{d_C\sqrt{3}}{4} - \frac{d_S\sqrt{3}}{3}\right) \quad (9)$$

$$\varepsilon_{PACKING} = 0.375 + 0.018\left(\frac{d_p}{d_W}\right) + 0.607\left(\frac{d_p}{d_W}\right)^2 \quad (10)$$

For R ≥5, the porosity data are essentially superimposed to the asymptotic porosity in packed bed reactors (i.e. 0.375), indicating that the presence of the POCS does not affect the catalyst packing. On decreasing R, until reaching the physical limit of R = 1 (below this limit, no catalyst can be packed in the POCS because the particles are bigger than the windows), the packing porosity progressively increases according to Eq. (10), indicating that some cavities in the POCS remain partially unfilled.

Using Eq. (10), a packing porosity of 0.41 is estimated in our case, which is 5 % lower than the value computed experimentally (0.43) and slightly higher than the asymptotic porosity in packed bed reactors. Such a value still indicates a very effective packing of the catalyst in the structured substrate, despite: (a) the additional packing obstacles represented by the presence of the outer and internal skins in the adopted POCS samples; (b) the value of R, which in our case is 4.9, i.e., only slightly below the threshold limit not to be affected by the effect of packing pellets [26]; (c) the PSD of the adopted catalyst micropellets, which may bring to packing efficiency somehow different from beds of pellets with uniform diameter.

3.3. Fischer-Tropsch runs

Fig. 4(a) shows, as a function of the Time-on-Stream (T.o.S.), the CO conversion and the CH_4 selectivity measured by progressively increasing the oil temperature from 180 °C to 225 °C, at 25 barg, GHSV = 4000 cm^3(STP)/h/g_{cat} and H_2/CO = 2.1 mol/mol.

CO conversion varies from less than 3 to over 70 %, quickly reacting to changes in the oil temperature and remaining stable in the entire investigated range. The same is true for methane selectivity, which grows from about 5 % to 10 % in the first 50 h, most probably due to the well-known catalyst reconstruction (or self-organization) when syngas is admitted to the reduced Co-catalyst [40–42], and then progressively grows from 10 % to 15 % upon increasing the oil temperature as typical of Co-based FTS catalysts.

The structured reactor quickly reacts also to changes in the GHSV (Fig. 4(b)), showing the expected decrease of the CO conversion and the expected minor increase of CH_4 selectivity upon increasing the space velocity. Again, the collected data demonstrate the excellent stability of the catalyst at CO conversions below 75 %, with the CO conversion starting to decrease with time only at GHSV = 3518 cm^3(STP)/h/g_{cat}, when CO conversions around 80 % were measured. This behaviour can be justified considering the very high P_{H2O}/P_{H2} reached at the reactor outlet [43], which is known to promote the oxidation of the Co^0 active sites to inactive CoO or Co_3O_4 species [44,45] and/or to the formation of FTS inactive cobalt-support mixed spinels [46,47].

Considering the outstanding catalyst stability, which is a first indirect indication of the efficient temperature control in the reactor, and the temperature sensitivity of the reactant conversion rate (the FTS has high activation energy, between 90 and 100 kJ/mol [32]) and of the product distribution [48], the average CO conversion and the average CH_4 and C_5 + selectivities in each condition, plotted in Fig. 5 against the oil temperature, will be used as such and to assess the quality of the heat transfer.

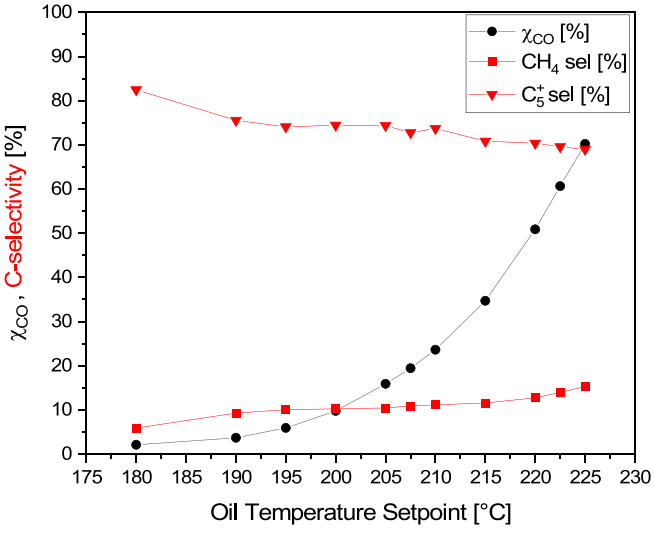

Fig. 5. CO conversion, CH_4 and C_{5+} selectivity as a function of the oil temperature at GHSV = 4000 cm^3(STP)/h/g_{cat}, P = 25 barg, H_2/CO = 2.1 mol/mol.

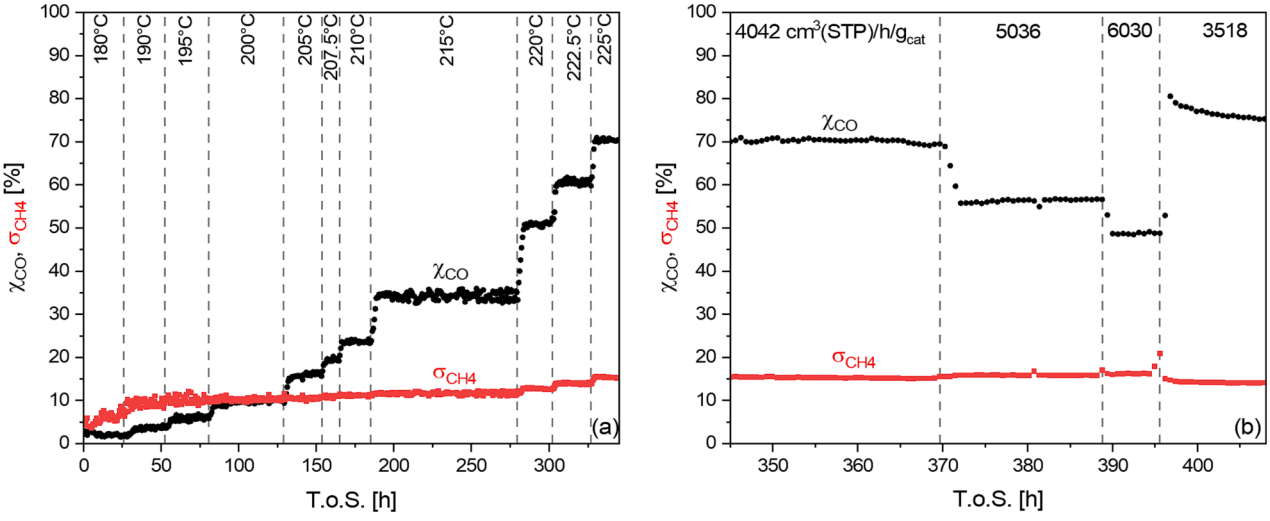

Fig. 4. CO conversion and CH_4 selectivity as a function of Time-on-Stream upon varying (a) the oil temperature at GHSV = 4000 cm^3(STP)/h/g_{cat} and (b) the GHSV at Toil = 225 °C. Other process conditions: P = 25 barg, H_2/CO = 2.1 mol/mol.

Notably, while the CO conversion increases exponentially with the temperature in the whole investigated temperature range, the CH_4 selectivity grows linearly up to 215 °C, showing only a weak dependence on temperature, and then grows slightly more rapidly at higher temperature. The C_{5+} selectivity mirrors the methane selectivity. As a consequence, the C_5 + yield increases exponentially with temperature (data not shown), exceeding 0.35 g/h/g_{cat} when the temperature of the oil was 225 °C. These data follow the trends typically observed during FTS kinetic measurements, in lab-scale reactors designed to be isothermal [49].

Fig. 6 shows the temperature profiles measured along the POCS axis during experiments at T_{oil} = 180, 200, 215 and 225 °C, along with the oil temperature upstream and downstream the catalyst bed and the five skin temperatures measured at different axial coordinates. Three profiles collected at each condition in a time span of 4 h are displayed, confirming that the catalyst was stable at each investigated conditions.

At each condition, the oil temperatures upstream and downstream the catalyst bed are coincident, and the wall temperatures measured along the axial coordinate only slightly deviate from the oil temperature. These data prove that the heat-transfer on the coolant side is highly efficient and has a minor impact on the observed temperature profiles in the catalyst bed. Notably, however, the temperature profiles measured along the catalyst-bed centerline are flat only at 180 °C (when CO conversion is about 3 %), but then evolve showing a hot-spot in the initial part of the catalyst bed.

To investigate this aspect further, Fig. 7(a) shows the effect of increasing the oil temperature (i.e., increasing CO conversion and heat duty, Fig. 7(b)) on the relative temperature increase in the reactor ($\Delta T = T_{cat} - T_{oil,avg}$), defined at each axial coordinate as the difference between the catalyst temperature on the reactor centerline and the average oil temperature.

A modest increase of temperature (≤2 °C) is observed in the first 25 mm of the structured catalyst bed when the coolant temperature is below or equal to 200 °C (CO conversion ≤10 %), which grows at 215 °C (CO conversion = 35 %), finally resulting in a marked hot-spot, located at z = 30 mm, at 225 °C (CO conversion = 70 %). This is due to the strong exothermicity of the FTS, which results in reaction duties in excess of 1 MW/m^3 at the highest investigated CO conversion level.

The shape of the profiles shown in Fig. 7(a) depends on a complex interplay between the reaction kinetics and the heat-transfer performance of the structured reactor. On one hand, in fact, all the profiles, are characterized by a sudden temperature increase at the catalyst bed inlet, a hot-spot in the first part of the bed, and then a progressive temperature decrease along the catalyst bed, which is typical of externally cooled packed-bed reactors with overall positive order kinetics with respect to the reactants: this is the case of the FTS [50–52]. Also, the fact that temperature profiles do not go back to the wall temperature at the reactor outlet is typical of the FTS kinetics, as the reaction rate is still significant even at CO conversion levels as high at 70 % (Fig. 8).

On the other hand, however, these profiles – characterized by a maximum temperature increase (ΔT_{max}) below 12 °C even at volumetric heat duties (Q_{vol}) in excess of 1 MW/m^3 Fig. 7(b)) – are due to the excellent heat transfer performances of the aluminium POCS with skin, which, thanks to the high effective radial conductivity and the tight contact with the tube wall, efficiently transfers the reaction heat from the catalyst bed to the reactor wall and then to the cooling oil.

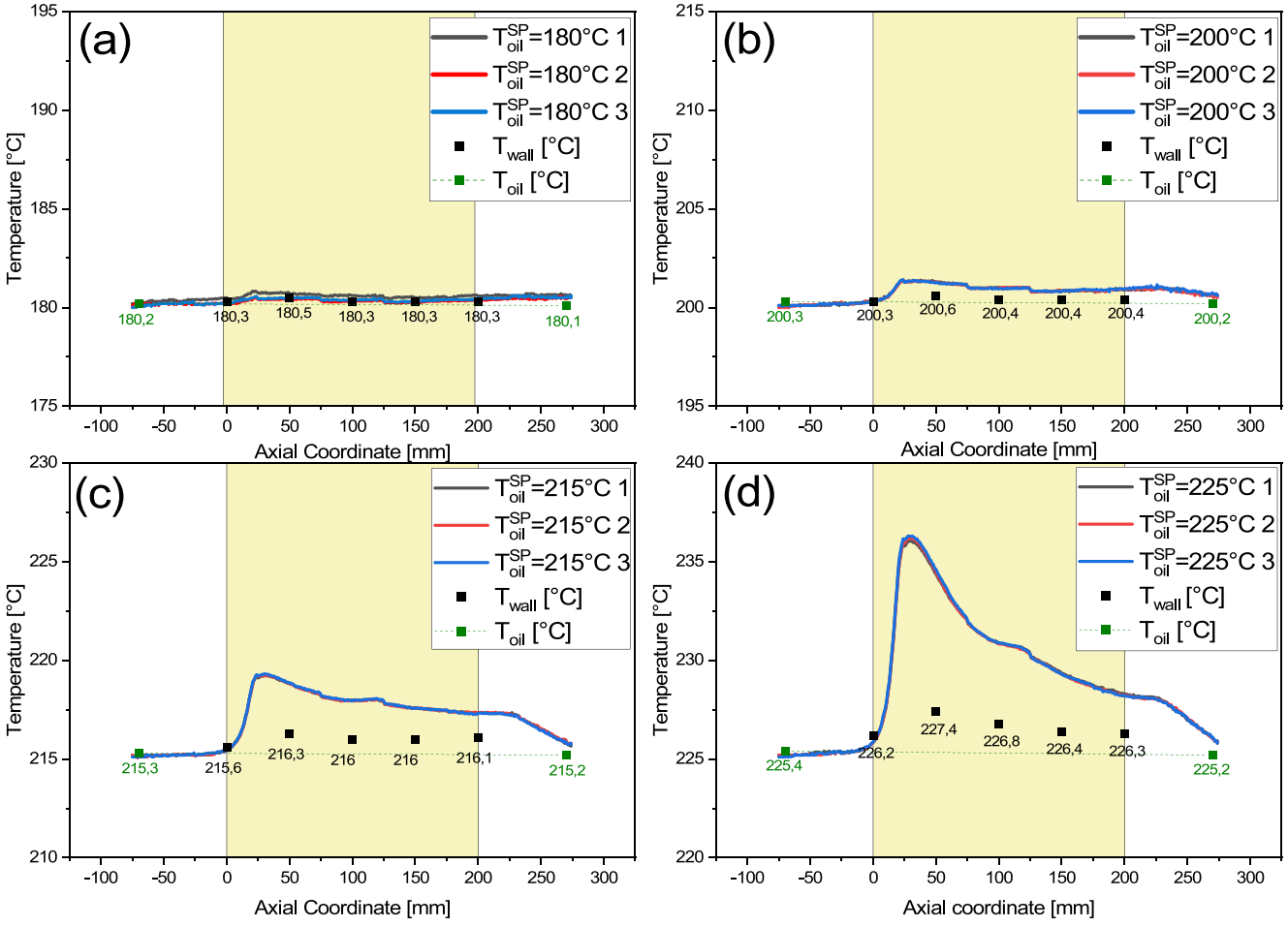

Fig. 6. Temperature profiles, skin temperature and oil temperature measured with an oil temperature set at (a) 180 °C; (b) 200 °C; (c) 215 °C; (d) 225 °C. Other process conditions: GHSV = 4000 cm^3(STP)/h/g_{cat}, P = 25 barg, H_2/CO = 2.1 mol/mol.

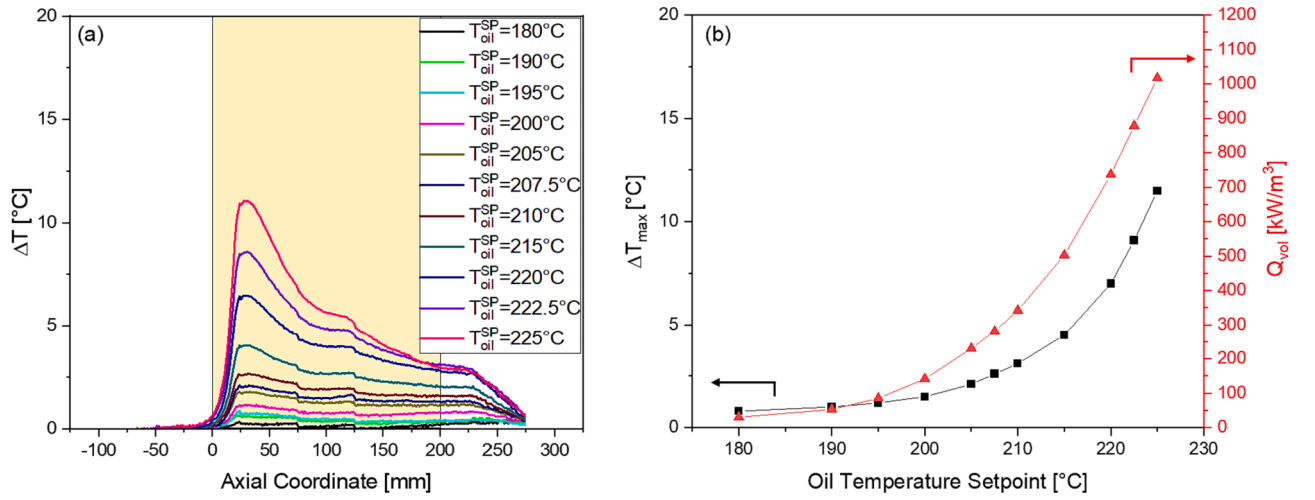

Fig. 7. Evolution of (a) the relative axial temperature increase in the reactor and (b) ΔT_{max} and Q_{vol} as a function of the oil temperature set-point. Other process conditions: GHSV = 4000 cm^3(STP)/h/g_{cat}, P = 25 barg, H_2/CO = 2.1 mol/mol.

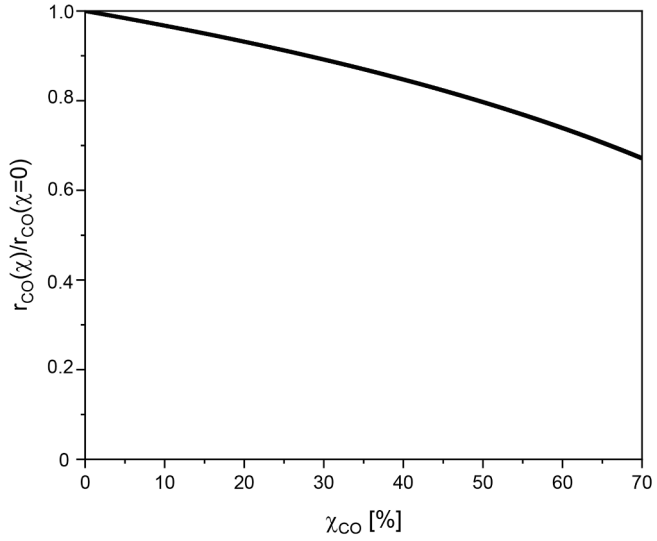

Fig. 8. Evolution of the normalized reaction rate with the CO conversion, according to the FTS kinetics reported in [51]. The simulation has been carried out at T = 230 °C, P = 25 bar, and H_2/CO = 2.1 mol/mol.

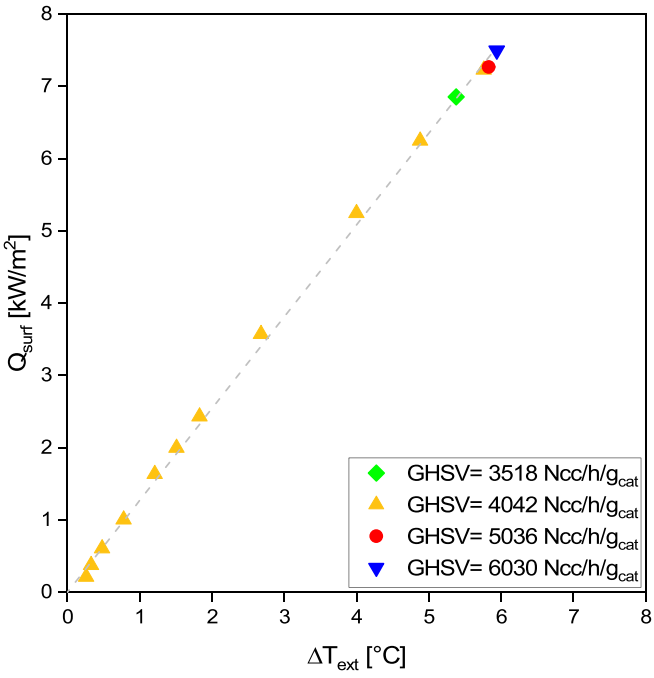

Fig. 9. Estimate of the overall heat transfer coefficient at different GHSV values. Experimental data collected at P = 25 bar and H_2/CO = 2.1 mol/mol, with the coolant kept at T_{oil} = 180–225 °C.

Fig. 9 shows the correlation between the heat flux (Q_{surf}, eq. (6)) and the difference between the average catalyst temperature on the centerline and the average oil temperature (ΔT_{ext}, eq. (7)) in each tested condition. Even if data have been collected almost doubling the gas velocity in the reactor between the low GHSV experiments and the high GHSV test, the experimental points are aligned along a single straight line. This confirms that the overall heat transfer coefficient is dominated by a flow-independent heat transfer mechanism, e.g. the static contribution to heat transfer from the pellets to the POCS solid lattice, the conduction within the thermally-connected solid matrix of the POCS and/or the contact resistance at the POCS skin-tube wall interface.

The slope of the straight line through the origin fitting the datapoints in Fig. 9 provides a conservative estimate of the overall heat transfer coefficient [24], as it refers to the maximum radial temperature difference: an outstanding value of ~1300 W/m^2/K is found for the tested configuration, which is far higher than typical overall heat transfer coefficients measured in very short packed-bed reactors (20 cm length).

The outstanding coefficient well explains the ability of the adopted reactor to manage the FTS with single-pass CO conversions in excess of 70 %, while granting an excellent control of the T-sensitive methane selectivity (always below 15 %) and exceptional catalyst stability even with a volumetric heat release exceeding 1 MW/m^3.

4. Conclusions

Aiming at maximising the atomic and energy efficiency of chemical processes, increasing catalyst stability and lifetime, reducing the environmental impact and the process footprint and improving the economics, one of the most relevant today's challenges of chemical reaction and process engineering is the intensification of heat transfer within catalytic reactors.

In this context, much interest lies in the optimization of compact non-adiabatic processes limited by the slow heat transfer from/to the catalyst. The convective mechanism dominating the heat-transfer in

large-scale tubular packed-bed reactors, in fact, becomes insufficient at the small scale (i.e. with short reactor tubes and small flowrates per tube), when the fluid velocities in the reactor are strongly decreased. Solid-phase heat conduction, in this case, can become game-changing.

In this paper, through Fischer-Tropsch runs carried out in a tailored pilot-scale plant installed in our labs, we have shown that a very efficient solution to intensify the heat-transfer in compact multi-tubular reactors is packing catalyst micro-pellets within highly conductive periodic-open-cellular-structures with skin. This solution mimics the highly conductive packed open-cell-foams we have been investigating during the last few years, but introduces the possibility to optimize the design of the cellular material, which is now manufactured by 3D printing, starting from a custom-made engineered model with almost no restrictions in terms of design.

In particular, we have demonstrated that exceptional overall heat transfer coefficients in excess of 1300 $W/m^2/K$ can be achieved using a packed-POCS with skin, allowing to manage the strong exothermicity and the high temperature sensitivity of the Fischer-Tropsch synthesis, even in a very short reactor. CO conversion levels in excess of 70 %, with CH_4 selectivity always below 15 % and C_{5+} specific yields in excess of 0.35 $g/h/g_{cat}$ have been achieved keeping the hotspot temperature rise below +12 °C from the coolant temperature, thus attenuating the strong temperature sensitivity typical of fixed-bed FT reactors.

These outstanding performances, among the best ever reported for a compact scale Fischer-Tropsch tubular reactor to our knowledge, are granted exclusively by the design of the adopted periodic open cellular structures, which are made of a highly-conductive aluminium alloy and are equipped with an external skin to maximise the contact at the interface between the POCS and the reactor.

The present results pave the way for the development of intensified multitubular fixed-bed reactor technologies for non-adiabatic applications at small scale, which are unfeasible today, while providing an alternative solution to micro-channel reactors which still relies on a well-established and proven reactor design.

Ongoing work is dedicated to investigating the role of the reactor and process design parameters in controlling the overall heat transfer performances of FTS tubular reactors. In particular, the relative contributions of the effective radial conductivity and of the wall heat transfer coefficient will be assessed, so to optimize the geometry of the POCS, minimizing its metal content while maximizing the catalyst inventory and the reactor yield.

Declaration of competing interest

The authors declare that they have no known competing financial interests or personal relationships that could have appeared to influence the work reported in this paper.

Data availability

Data will be made available on request.

Acknowledgments

This project has received funding from the European Research Council (ERC) under the European Union's Horizon 2020 research and innovation programme (grant agreement No 694910 – INTENT).

References

[1] F. Kapteijn, J.A. Moulijn, Catalysis Today 383 (2022) 5–14.
[2] M. Sheng, H. Yang, D.R. Cahela, B.J. Tatarchuk, Journal of Catalysis 281 (2011) 254–262.
[3] E. Tronconi, G. Groppi, C.G. Visconti, Current Opinion in Chemical Engineering 5 (2014) 55–67.
[4] A. Cybulski, J.A. Moulijn, Structured Catalysts and Reactors, Marcel Dekker, New York, 1998.
[5] J.R. Van Ommen, J.A. Moulijn, F. Kapteijn, Catalysis Science and Technology 5 (2015) 807–817.
[6] T.A. Nijhuis, A.E.W. Beers, T. Vergunst, I. Hoek, F. Kapteijn, J.A. Moulijn, Catalysis Reviews - Science and Engineering 43 (2001) 345–380.
[7] A. Montebelli, C.G. Visconti, G. Groppi, E. Tronconi, C. Cristiani, C. Ferreira, S. Kohler, Catalysis Science and Technology 4 (2014) 2846–2870.
[8] E. Tronconi, G. Groppi, T. Boger, A.K. Heibel, Chemical Engineering Science 59 (2004) 4941–4949.
[9] C.G. Visconti, E. Tronconi, G. Groppi, L. Lietti, M. Iovane, S. Rossini, R. Zennaro, Chemical Engineering Journal 171 (2011) 1294–1307.
[10] D. Merino, O. Sanz, M. Montes, Chemical Engineering Journal 327 (2017) 1033–1042.
[11] L. Giani, G. Groppi, E. Tronconi, Industrial and Engineering Chemistry Research 44 (2005) 9078–9085.
[12] A. Aguirre, E. Scholman, J. van der Shaaf, M. Fernanda Neira d'Angelo,, Chemical Engineering Journal 409 (2021) 128139.
[13] Y. Wang, D.P. VanderWiel, A.L.Y. Tonkovich, Y. Gao, E.G. Baker, inventors; Battelle Memorial Institute Inc, applicant. Catalyst structure and method of Fischer-Tropsch synthesis, US6451864.
[14] C. Cao, J. Hu, S. Li, W. Wilcox, Y. Wang, Catalysis Today 140 (2009) 149–156.
[15] R. Myrstad, S. Eri, P. Pfeifer, E. Rytter, A. Holmen, Catalysis Today 147S (2009) S301-S304.
[16] M. Iovane, R. Zennaro, G. Groppi, L. Lietti, E. Tronconi, C.G. Visconti, S. Rossini, E. Mignone, inventors; Eni S.p.A., applicant. Reactor for exothermic and endothermic catalytic reactions. Patent application WO/2010/130399.
[17] M. Paturzo, M. Favaretto, M. Piazza, P. Forzatti, G. Groppi, L. Lietti, E. Tronconi, C. G. Visconti, inventors; Eni S.p.A., applicant. Multi-structured reactor made of monolithic adjacent thermoconductive bodies for chemical processes with a high heat exchange. Patent application WO/2014/102350.
[18] M. Sheng, H. Yang, D.R. Cahela, W.R. Yantz Jr., C.F. Gonzalez, B.J. Tatarchuk, Applied Catalysis a: General 445–446 (2012) 143–152.
[19] A.E. Abusrafa, M.S. Challiwala, B.A. Wilhite, N.O. Elbashir, Processes 8 (2020) 1213.
[20] D. Vervloet, F. Kapteijn, J. Nijenhuis, J.R. van Ommen, Catalysis Today 216 (2013) 111–116.
[21] T.J. Schildhauer, K. Pangarkar, J.R. van Ommen, J. Nijenhuis, J.A. Moulijn, F. Kapteijn, Chemical Engineering Journal 185–186 (2012) 250–266.
[22] J.L. Barrera, J.J. Hartvigsen, M. Hollist, J. Pike, A. Yarosh, N.P. Fullilove, V. A. Beck, Chemical Engineering Science 268 (2023) 118423.
[23] G. Groppi, E. Tronconi, C.G. Visconti, A. Tasso, R. Zennaro, inventors; Eni S.p.A., applicant. Packed-bed tubular reactor for heterogeneous exothermic or endothermic catalytic reactions. Patent application WO/2015/033266.
[24] L. Fratalocchi, G. Groppi, C.G. Visconti, L. Lietti, E. Tronconi, Chemical Engineering Journal 386 (2020) 123988.
[25] C.G. Visconti, G. Groppi, E. Tronconi, Catalysis Today 273 (2016) 178–186.
[26] M. Ambrosetti, G. Groppi, W. Schwieger, E. Tronconi, H. Freund, Chemical Engineering and Processing - Process Intensification 155 (2020) 108057.
[27] A. Inayat, J. Schwerdtfeger, H. Freund, C. Körner, R.F. Singer, W. Schwieger, Chemical Engineering Science 66 (2011) 2758–2763.
[28] M. Klumpp, A. Inayat, J. Schwerdtfeger, C. Körner, R.F. Singer, H. Freund, W. Schwieger, Chemical Engineering Journal 242 (2014) 364–378.
[29] M. Bracconi, M. Ambrosetti, M. Maestri, G. Groppi, E. Tronconi, Chemical Engineering and Processing – Process Intensification 158 (2020) 108169.
[30] E. Bianchi, W. Schwieger, H. Freund, Advanced Engineering Materials 18 (2016) 608–614.
[31] B. Sarup, B.W. Wojciechowski, Canadian Journal of Chemical Engineering 67 (1989) 62–74.
[32] I.C. Yates, C.N. Satterfield, Energy & Fuels 5 (1991) 168–173.
[33] C.G. Visconti, L. Lietti, E. Tronconi, P. Forzatti, R. Zennaro, S. Rossini, Catalysis Today 154 (2010) 202–209.
[34] C.G. Visconti, E. Tronconi, L. Lietti, P. Forzatti, S. Rossini, R. Zennaro, Topics in Catalysis 54 (2011) 786–800.
[35] L. Fratalocchi, C.G. Visconti, G. Groppi, L. Lietti, E. Tronconi, Chemical Engineering Journal 349 (2018) 829–837.
[36] L. Fratalocchi, G. Groppi, C.G. Visconti, L. Lietti, E. Tronconi, Reaction Chemistry & Engineering 4 (2019) 1917–1921.
[37] L. Fratalocchi, G. Groppi, C.G. Visconti, L. Lietti, E. Tronconi, Catalysis Today 383 (2022) 15–20.
[38] C. Ferroni, M. Bracconi, M. Ambrosetti, M. Maestri, G. Groppi, E. Tronconi, Industrial & Engineering Chemistry Research 60 (2021) 10522–10538.
[39] M. Lammermann, G. Horak, W. Schwieger, H. Freund, Chemical Engineering and Processing – Process Intensification 126 (2018) 178–189.
[40] H. Schulz, Applied Catalysis A 186 (1999) 3–12.
[41] H. Schulz, Topics in Catalysis 26 (2003) 73–85.
[42] A.Y. Khodakov, W. Chu, P. Fongarland, Chemical Reviews 107 (2007) 1692–1744.
[43] L. Fratalocchi, C.G. Visconti, L. Lietti, G. Groppi, E. Tronconi, E. Roccaro, R. Zennaro, Catalysis Science & Technology 6 (2016) 6431–6440.
[44] E.A. Blekkan, O. Borg, V. Froseth, A. Holmen, Catalysis 20 (2007) 13–32.
[45] N. Fischer, B. Clapham, T. Feltes, M. Claeys, ACS Catalysis 5 (2015) 113–121.
[46] A.K. Dalai, B.H. Davis, Applied Catalysis A 348 (2008) 1–15.
[47] D.J. Moodley, A.M. Saib, J. van de Loosdrecht, C.A. Welker-Nieuwoudt, B. H. Sigwebela, J.W. Niemantsverdriet, Catalysis Today 171 (2011) 192–200.
[48] A.O. Odunsi, T.S. O'Donovan, D.A. Reay, Applied Thermal Engineering 93 (2016) 1377–1393.
[49] H. Schulz, E. van Steen, M. Claeys, Studies in Surface Science and Catalysis 81 (1994) 455–460.

[50] R. Zennaro, M. Tagliabue, C.H. Bartholomew, Catalysis Today 58 (2000) 309–319.
[51] C.G. Visconti, M. Mascellaro, Catalysis Today 214 (2013) 61–73.
[52] K. Keyvanloo, S.J. Lanham, W.C. Hecker, Catalysis Today 270 (2016) 9–18.